Unique Expansion of PARP Family Proteins in the *Fusarium oxysporum* species complex

Cecelia Murphy*, Shira Milo*, Dan Norment, Houlin Yu, Domingo Martinez-Soto, and Li-Jun Ma

*denotes equal contribution

UMassAmherst | College of Natural Sciences, Center for Agriculture, Food, and the Environment

NIH National Institutes of Health

Background

The versatile poly-ADP ribose polymerase (PARP) protein family participates in numerous cellular functions, including DNA repair, apoptosis, chromatin remodeling, and cell cycle regulation[2]. PARPs create long chains of ADP-riboses as they transfer ADP-ribose from NAD^+ to their own amino acid residues or other acceptor molecules in a process called PARylation[2]. PARP1 has been thoroughly characterized in humans as the primary DNA repair PARP that senses DNA damage sites and recruits downstream DNA repair proteins, however the roles of PARP1 and the rest of the PARP family members are yet to be fully characterized in filamentous fungi[4]. Comparative genomic analysis revealed that the PARP family is uniquely expanded in the *Fusarium oxysporum* species complex, a filamentous fungus best known for agriculturally devastating crops such as bananas and tomatoes, causing enormous economic losses. PARP family genes are located on both the highly conserved core genome and the flexible, strain-specific accessory chromosomes of the *F. oxysporum* genome[7] with copy number ranges from three to twenty across strains. In this study, four strains of *F. oxysporum* that possess different numbers of PARP proteins are used as a comparative system: Fo47, an endophyte; Fol4287, a tomato pathogen; MRL8996, a human pathogen; and Fo5176, an *Arabidopsis* pathogen. Infecting tomato plants, mice, and *Arabidopsis* with wild-type and *Parp1*-deficient *F. oxysporum* strains allows for the assessment of the impact of PARP1 on fungal disease cycle. Optimizing quantification of PARylated proteins under DNA damage conditions by Western Blot allows for future investigation into levels and effect of PARP copy number on cellular PARylation.

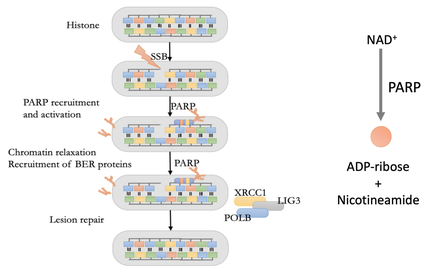

PARP Family Repertoire

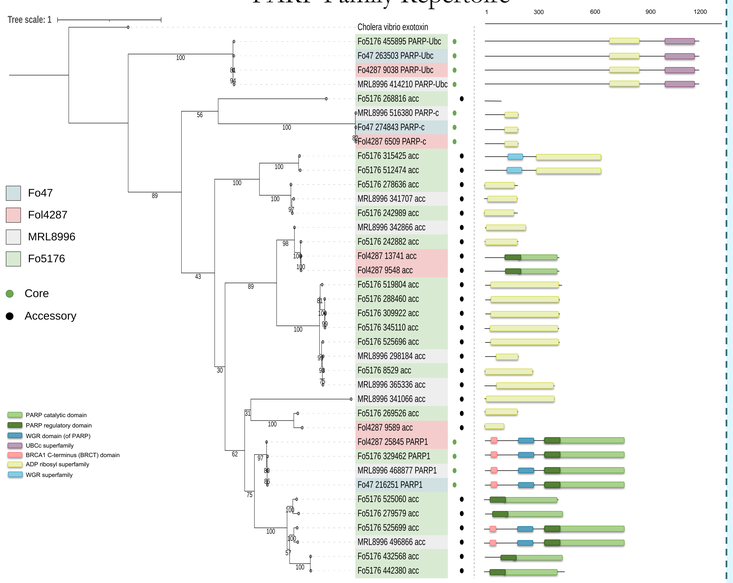

Figure 1. Phylogenetic Trees and Conserved Domain Annotations.
PARP sequences were aligned and corrected using MAFFT [5] and and Noisy[1]. Phylogenetic trees were generated using IQ-TREE[8] for tree construction, and ITOL[5] for visualization. Conserved domains were identified using the NCBI CDD Tool[6]. The four strains from the comparative system are shown above: A) the Fo47, 3 PARPs, B) the Fol4287, 6 PARPs, C) the MRL8996, 9 PARPs, and D) the Fo5176, 20 PARPs.

PARP Family Expansion Across the Fungal Kingdom

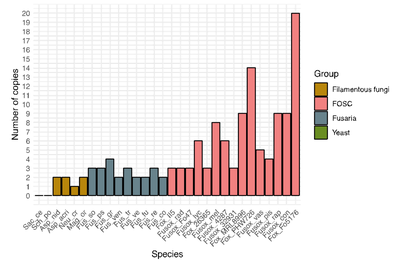

Figure 2. Number of Parp copies across the fungal kingdom.
PARP copy numbers across several fungal phylogenetic groups, including the FOSC, shown in pink. Analysis and visuals by Shira Milo.

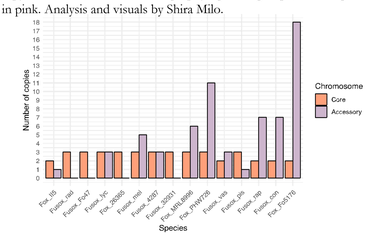

Figure 3. Distribution of PARP family members across FOSC core and accessory chromosomes. Genomic location of different PARP genes within the FOSC. Core chromosomes are shown in orange while accessory chromosomes are shown in lilac. Analysis and visuals by Shira Milo.

PARP copy number is positively correlated with DNA damage tolerance

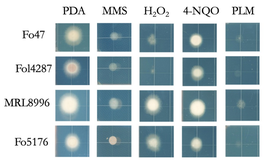

Figure 4. DNA damage tolerance (survival) in *F. oxysporum* WT strains
10^4, 10^3, and 10^2 cells of each strain were plated on potato dextrose agar (PDA) containing MMS, H_2O_2, 4-NQO, or phleomycin (PLM). MMS and H_2O_2 damage is mainly repaired by the base excision repair pathway while 4-NQO is exclusively repaired by the nucleotide excision repair pathway. Phleomycin causes double strand breaks in DNA, mainly repaired by homologous recombination and non homologous end-joining.

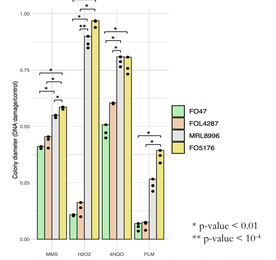

Figure 5. Colony Diameter of *F. oxysporum* WT strains under DNA damage conditions.
Colony diameter ratios were calculated by dividing the size of a colony under a DNA damage condition by the size of the corresponding control colony plated on PDA. Colony diameter ratios were measured for plates containing MMS, H_2O_2, 4-NQO, or phleomycin (PLM). Analysis and visuals by Shira Milo.

Generating *Parp1*-deficient strains

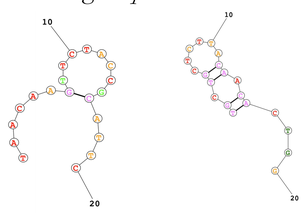

Position: 821
On-target score: 43.5
Off-target score: 49.8

Position: 1923
On-target score: 66.6
Off-target score: 49.6

Figure 6. Predicted secondary structures for CRISPR RNA (crRNA) used in MRL8996 *Parp1* knockout.
Images were generated using the Mathews Lab online RNAstructure tool[9] Secondary structure formation probability was <50% for crRNAs at positions 821 and 1923.

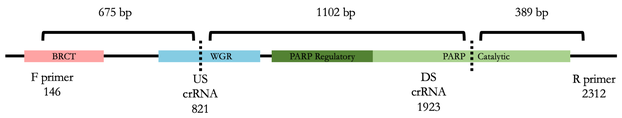

Figure 7. MRL8996 *Parp1* crRNA cut sites.
crRNA were designed to cut the *Parp1* gene at nucleotides 821 and 1923, creating three fragments and allowing for the insertion of a Hygromycin B resistance gene in place.

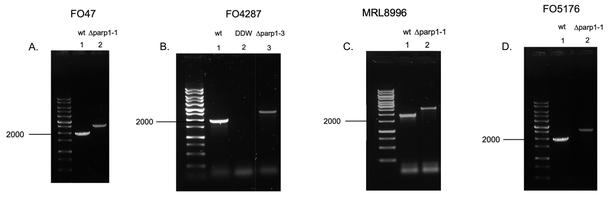

Figure 8. PCR validation of suspected *Parp1*-deficient strains.
Suspected mutants in the A) Fo47, B) Fol4287, C) MRL8996, and D) Fo5176 strains were PCR analyzed and compared to their wild-type *Parp1* gene to confirm insertion of the Hygromycin B gene. Confirmation of the Hygromycin B inserts by Sanger Sequencing was additionally performed.

In planta Phenotyping

Figure 9. *Arabidposis* plants 10 days post infection.
Arabidopsis plants were inoculated in *F. oxysporum* spore solution for 90 minutes and grown for 10 days. A) Plants infected with WT or *Parp1*-mutant of the endophyte Fo47, B) Plants infected with WT or *Parp1*-mutant of the pathogen Fo5176.

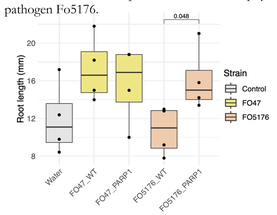

Figure 10. *Arabidopsis* root length 10 dpi.
Root lengths were measured in millimeters and statistical analyses were performed, with a cutoff of p-value<0.05 between WT and *Parp1*-deficient strains (Fo47, Fo5176).

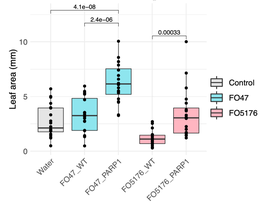

Figure 11. *Arabidopsis* leaf area 10 dpi.
Leaf area was measured in millimeters and statistical analyses were performed, with a cutoff of p-values<0.05 between WT and *Parp1*-deficient strains (Fo47, Fo5176).

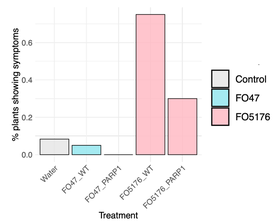

Figure 12. Number of *Arabidopsis* plants showing symptoms 10 dpi.
The percentage of plants in each treatment showing symptoms.

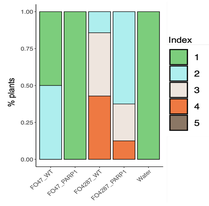

Figure 13. Disease index of tomato plants infected with WT and Parp1-deficient strains (Fo47, Fol4287) measured 4 dpi.
Disease index assessment performed by Domingo Martinez-Soto.

Protein Extraction Calibration and Optimization

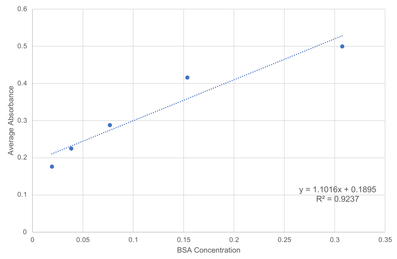

Figure 14. Deriving a standard curve to calculate protein concentration.
Crude protein extract sample concentrations were determined by plotting absorbances of bovine serum albumin (BSA) samples against their known concentrations. The standard curve was used to calculate the concentration of crude protein extracts from *F. oxysporum*.

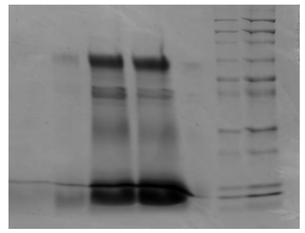

Figure 15. Visualization of crude protein extract.
Wild-type Fol4287 samples, were visualized in SDS-PAGE gel using electrophoresis.

Future directions

1) Repeat *Arabidopsis* infections using ROS-deficient *Arabidopsis* plants to better understand the role of PARP1 during plant colonization/infection.

2) Study PARylation trends in all wild type strains and mutants included in our comparative system using Western blot.

3) Investigate the role of PARP-Ubc by knocking out the gene and characterizing the mutants.

References

[1] Dress, A. W., Flamm, C., Fritzsch, G., Grünewald, S., Kruspe, M., Prohaska, S. J., & Stadler, P. F. (2008). Noisy: Identification of problematic columns in multiple sequence alignments. *Algorithms for Molecular Biology*, *3*(1), 7. https://doi.org/10.1186/1748-7188-3-7

[2] Kamaletdinova, T., Fanaei-Kahrani, Z., & Wang, Z.-Q. (2019). The Enigmatic Function of PARP1: From PARylation Activity to PAR Readers. *Cells*, *8*(12), 1625. https://doi.org/10.3390/cells8121625

[3] Katoh, K., & Standley, D. M. (2013). MAFFT Multiple Sequence Alignment Software Version 7: Improvements in Performance and Usability. *Molecular Biology and Evolution*, *30*(4), 772–780. https://doi.org/10.1093/molbev/mst010

[4] Lan, L., Nakajima, S., Oohata, Y., Takao, M., Okano, S., Masutani, M., Wilson, S. H., & Yasui, A. (2004). In situ analysis of repair processes for oxidative DNA damage in mammalian cells. *Proceedings of the National Academy of Sciences*, *101*(38), 13738–13743. https://doi.org/10.1073/pnas.0406048101

[5] Letunic, I., & Bork, P. (2021). Interactive Tree Of Life (iTOL) v5: An online tool for phylogenetic tree display and annotation. *Nucleic Acids Research*, *49*(W1), W293–W296. https://doi.org/10.1093/nar/gkab301

[6] Lu, S., Wang, J., Chitsaz, F., Derbyshire, M. K., Geer, R. C., Gonzales, N. R., Gwadz, M., Hurwitz, D. I., Marchler, G. H., Song, J. S., Thanki, N., Yamashita, R. A., Yang, M., Zhang, D., Zheng, C., Lanczycki, C. J., & Marchler-Bauer, A. (2020). CDD/SPARCLE: The conserved domain database in 2020. *Nucleic Acids Research*, *48*(D1), D265–D268. https://doi.org/10.1093/nar/gkz991

[7] Ma, L.-J., van der Does, H. C., Borkovich, K. A., Coleman, J. J., Daboussi, M.-J., Di Pietro, A., Dufresne, M., Freitag, M., Grabherr, M., Henrissat, B., Houterman, P. M., Kang, S., Shim, W.-B., Woloshuk, C., Xie, X., Xu, J.-R., Antoniw, J., Baker, S. E., Bluhm, B. H., … Rep, M. (2010). Comparative genomics reveals mobile pathogenicity chromosomes in Fusarium. *Nature*, *464*(7287), 367–373. https://doi.org/10.1038/nature08850

[8] Nguyen, L.-T., Schmidt, H. A., von Haeseler, A., & Minh, B. Q. (2015). IQ-TREE: A Fast and Effective Stochastic Algorithm for Estimating Maximum-Likelihood Phylogenies. *Molecular Biology and Evolution*, *32*(1), 268–274. https://doi.org/10.1093/molbev/msu300

[9] Reuter, J. S., & Mathews, D. H. (2010). RNAstructure: Software for RNA secondary structure prediction and analysis. *BMC Bioinformatics*, *11*(1), 129. https://doi.org/10.1186/1471-2105-11-129

Acknowledgements

Shira, thank you for your never-ending support and kindness. Our second summer working together holds a special place in my heart, and I will carry all the lessons you taught me as I continue to learn and grow as a scientist.
Domingo, thank you for your guidance through the *in planta* and Western Blot processes. I so appreciate the hours you've dedicated to teaching me and always encouraging me to challenge myself.
Professor Ma, thank you for the opportunity to continue my education this summer, and for your encouragement throughout.
Thank you to the entire Ma lab for creating such a positive and enjoyable work environment.
This project was supported by the National Eye Institute of the National Institutes of Health under award number: R01EY030150.